# Development and evaluation of a many-electron–multicenter classical-trajectory Monte Carlo model in charge-exchange processes involving collisions of multiply charged ions and CO

N. D. Cariatore and S. Otranto

*IFISUR and Departamento de Física, Universidad Nacional del Sur, 8000 Bahía Blanca, Argentina*

A many-electron–multicenter classical-trajectory Monte Carlo model is developed and tested in charge-exchange studies involving projectiles with charges from $+3$ to $+10$ and the CO molecule. The present model is contrasted against simpler single-center and independent-atom approaches. Total and state-selective charge-exchange cross sections are presented and are compared to recent data from the Jet Propulsion Laboratory where available.

## I. INTRODUCTION

In the past few years, the need for charge-exchange data and line emission cross sections in astrophysical and biological environments has pushed the existing theoretical models (based on either classical, semiclassical, or quantum mechanical grounds) to their limits [1–10]. Accurate charge-exchange and ionization databases are required to achieve a precise interpretation of photonic spectra in astrophysical environments, and to correctly infer the energy deposition in ion-beam radiotherapy.

Molecules, in this sense, represent targets that are much more complex to characterize than atoms. Besides the interelectronic interactions, the multicenter nature of the target represents an additional challenge, especially at low impact energies at which the electrons are shared by two or more heavy centers (including the projectile, in case it turns out to be an ion). In addition, competing molecular orbitals with similar ionization potentials centered on separate nuclei provide alternative energetic routes for a given process to take place.

State-selective charge-exchange processes between charged ions and different atomic and molecular targets, and their eventual subsequent radiative decays, have been systematically explored at JPL, KVI, LLNL-EBIT, NIST-EBIT, the University of Reno, and Berlin-EBIT during the past decade [2,6,7,11–18]. Although these combined efforts are still far from providing a complete description of the underlying physics, they provide concrete tests which allow one to evaluate the performance of the current theoretical models.

In this sense, quantum mechanical theoretical efforts have mainly focused on the hydrogen target [19,20] by using expansions in terms of atomic or molecular orbitals. The drastic enhancement in the basis size required as the projectile charge increases represents the main obstacle and results in larger computational times. Simpler models such as the multichannel Landau-Zener [21], the classical-over-the-barrier [22], and the classical-trajectory Monte Carlo (CTMC) method [23,24], on the other hand, provide faster access to state-selective charge-exchange data and as a result have been widely employed in the field during the past two decades. However, in most cases, datasets have been generated with these models under the hydrogenic approximation (i.e., a hydrogen atom for which the ionization potentials are varied). Very recently, Illescas

*et al.* introduced a multicenter model for the H$_2$O molecule which considers a single active electron [25]. The authors tested this model up to the total cross-section level for the charge-exchange, ionization, and electron-loss channels. In this sense, up to our knowledge, many-electron–multicenter CTMC codes for molecular targets beyond H$_2$ [26,27] are not readily available in the literature.

With the aim of exploring a more realistic representation of the collision process, in this work we develop a many-electron–multicenter CTMC approach (hereafter referred to as mmCTMC). In particular, this model will be tested in the framework of charge-exchange processes between ions with charges $+3$ and $+10$ and CO molecules for which we consider 8-active electrons. This many-electron treatment allows estimating the contribution of the autoionizing multiple charge-exchange channel to the single charge-exchange cross sections. In contrast, one-electron treatments indirectly predict multiple capture cross sections by recalling typical binomial distributions [25,28,29].

The results obtained with the present model are contrasted to those obtained by an eight-electron–single-center CTMC model as well as to those obtained by means of the independent-atom approximation. Recent experimental data obtained at JPL (total and state-selective charge-exchange cross sections) will be used to evaluate the performance of these theoretical models where available.

## II. THEORETICAL MODELS

In what follows, we introduce the CTMC models that are used throughout this work.

*mmCTMC.* In this model the two ionic centers are fixed in space at the equilibrium distance which for CO is given by $R = 2.13$ a.u.. The molecular axis is randomly oriented and the eight electrons interact with both centers via the pseudopotential developed by Gabas *et al.* [30]:

$$V(r_{eC}, r_{eO}) = V_O(r_{eO}) + V_C(r_{eC}),$$

$$V_O(r_{eO}) = -\frac{8 - N_O}{r_{eO}} - \frac{N_O}{r_{eO}}(1 + \alpha_O r_{eO})e^{-2\alpha_O r_{eO}}, \quad (1)$$

$$V_C(r_{eE}) = -\frac{6 - N_C}{r_{eC}} - \frac{N_C}{r_{eC}}(1 + \alpha_C r_{eC})e^{-2\alpha_C r_{eC}}.$$

The corresponding coefficients are $N_O = 7.609$, $N_C = 5.391$, $\alpha_O = 1.501$, and $\alpha_C = 0.85$.
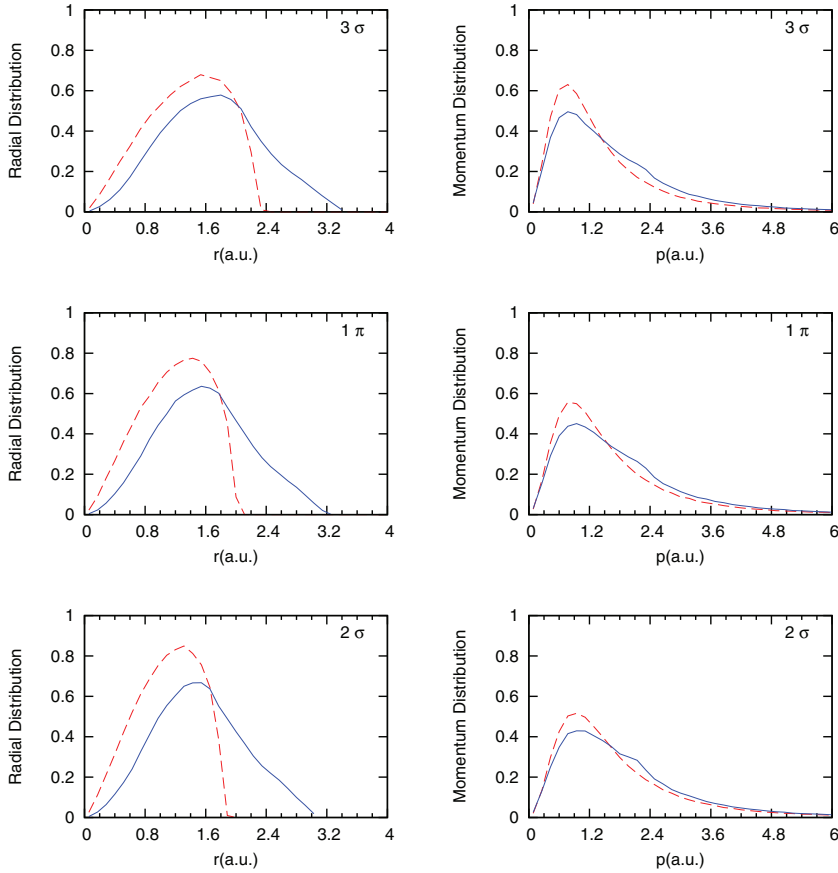
FIG. 1. (Color online) Radial and momentum distributions (left and right columns, respectively) corresponding to the SC (dashed red line) and mmCTMC (solid blue line) models for the three molecular orbitals under consideration. Solid line: mmCTMC; dashed line: SC model.

The eight electrons are randomly sorted in the energetically allowed region surrounding the molecular nuclei. Two electrons are sorted with an ionization potential (IP) of 14.01 eV ($3\sigma$ orbital), four electrons are sorted with an IP of 17.4 eV ($1\pi$ orbital), and two electrons are sorted with an IP of 19.88 eV ($2\sigma$ orbital).

*Single-center model (SC)*. This model has been used by Simcic *et al.* [7] and consists in approximating the CO molecule by the atomic dominant element (oxygen) with eight active electrons. The electrons interact with the parent nucleus via the Garvey central potential [31]

$$V(r) = -\frac{Z - (N - 1)[1 - \Omega(r)]}{r},$$
$$\Omega(r) = \left[\left(\frac{\eta}{\xi}\right)(e^{\xi r} - 1) + 1\right]^{-1}. \quad (2)$$

For $O^+$, the involved parameters are given by $Z = 8$, $N = 8$, $\xi = 1.36$, $\eta = 2.41$. As in the former case, two electrons are sorted with an IP of 14.01 eV, four electrons are sorted with an IP of 17.4 eV, and two electrons are sorted with an IP of 19.88 eV.

*Independent atoms (IA)*. In this model, the two ionic centers are fixed in space at the equilibrium distance $R = 2.13$ a.u.. The electrons are sorted in separate $C^+$ and $O^+$ centers based on the population scheme developed by Mulliken [32]. In this sense, each electron is forced to see a single target ionic core (either $C^+$ or $O^+$) throughout the collision. Three electrons are then bound to the $C^+$ ion with ionization potentials of 14.01 eV (two electrons) and 17.4 eV (one electron). The five remaining electrons are attached to the $O^+$ ion with ionization potentials of 17.4 eV (three electrons) and 19.88 eV (two electrons). The electrons interact respectively with the $C^+$ or $O^+$ centers via Garvey potentials [31]. For $C^+$ the corresponding parameters read $Z = 6$, $N = 6$, $\xi = 1.065$, $\eta = 2.13$.

Throughout the years different strategies have been conceived within the CTMC in order to include the interelectronic interaction for two-electron systems. We can cite the Heisenberg core technique introduced by Kirchbaum and Wilets [33], the dynamical screening model (dCTMC) of Montemayor and Schiwietz [34], and the Bohr atom of Olson [35], among others. Although more refined treatments could possibly consider dynamical screenings to partially account for the interelectronic interactions in the present model, these are, however, beyond the scope of the present article. Hence, in all cases, the interelectronic interactions among electrons are not included to avoid the classical autoionization of the target.

In Fig. 1, we show and compare the momentum and radial distributions obtained with the SC and mm CTMC models after sorting $3 \times 10^5$ trajectories. The molecular orientation is randomly sorted for each considered trajectory. Despite the fact that the momentum distributions for the different electrons are quite similar for these treatments, clear differences are observed between the respective radial distributions (note that the random orientation of the molecular axis leads to spherical distributions for the mmCTMC model).

The SC distributions show the drastic falloff at the classical return point, typical of the microcanonical distribution. The mmCTMC distributions, on the other hand, preserve a width
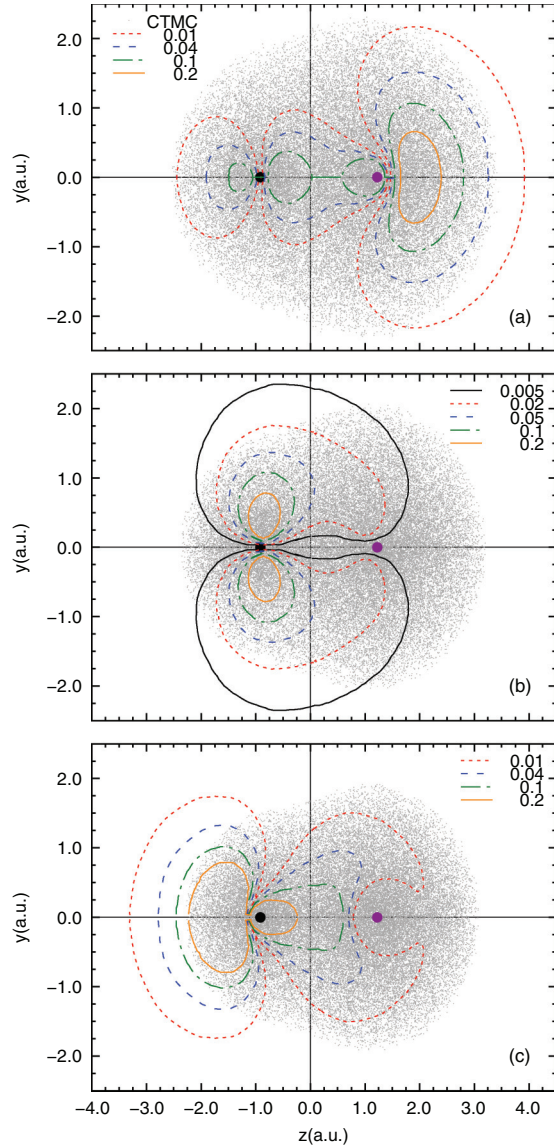
FIG. 2. (Color online) mmCTMC electronic density plot for the three main molecular orbitals of the CO molecule: (a) $3\sigma$, (b) $1\pi$, (c) $2\sigma$. The $z$ axis represents the molecular axis and the O and C ionic centers are explicitly indicated (left and right, respectively). In all cases contours obtained by Huo [36] based on the wave function obtained with the self-determinantal self-consistent field method are included.

in the distribution (or radial extension) related to the nuclei separation. To further highlight this point, in Fig. 2 we show a scatter plot of the sorted position in the $z$-$y$ plane (where $z$ is the molecular axis) for the active electrons. This electronic density plots provide a clear view of the energetically allowed region. The contour lines of Huo based on the self-determinantal, self-consistent field method [36] are included for comparison.

### A. State-selective cross sections

The final state population $(n,l,m)$ associated to a particular charge-exchange event is characterized according to the standard Becker and McKellar binning rule [37]

$$[n(n - 1/2)(n - 1)]^{1/3} \leqslant n_c < [n(n + 1/2)(n + 1)]^{1/3}, \quad (3)$$

together with [38]

$$l \leqslant l_c < l + 1,$$
$$\frac{2m_l - 1}{2l + 1} \leqslant \frac{l_z}{l_c} \leqslant \frac{2m_l + 1}{2l + 1}, \quad (4)$$

where $\boldsymbol{l}_c = (n/n_c)(\boldsymbol{r} \times \boldsymbol{k})$ and $\boldsymbol{r}$ and $\boldsymbol{k}$ are the position and momentum of the electron relative to the projectile. The charge-exchange cross section of P electrons to the state $(\boldsymbol{n},\boldsymbol{l},\boldsymbol{m}) = (n_1, n_1, \ldots, n_P, l_1, l_2, \ldots, l_P, m_1, m_2, \ldots, m_P,)$ is given by

$$\sigma_{nlm} = \frac{N(\boldsymbol{n},\boldsymbol{l},\boldsymbol{m})}{N_{\text{tot}}} \pi b_{\text{max}}^2, \quad (5)$$

where $N(\boldsymbol{n},\boldsymbol{l},\boldsymbol{m})$ is the number of electron capture events to the $\boldsymbol{nlm}$ state and $N_{\text{tot}}$ is the total number of trajectories considered. The maximum impact parameter contributing to electron capture is denoted as $b_{\text{max}}$.

For partially stripped projectiles these binning rules are modified following the methodology proposed by Pascale *et al.* [39], which defines an effective quantum number $n$ by incorporating electronic quantum defects. In addition, capture events which populate any completely filled shell are neglected.

Provided that multiple capture can technically involve up to eight electrons, an *ab initio* treatment of the Auger decay dynamics based on individual rates is not feasible. In all cases, multiple electron capture will be treated according to the decay scheme developed by Ali *et al.* [40] for collisions involving argon ions with argon atoms which can be summarized as follows:

 (i) Multiply excited states dominantly stabilize via multiple Auger processes.

 (ii) Two-electron Auger processes are considered only.

 (iii) Transitions involving electrons in the same shell proceed first. If several electrons are in different shells, the Auger process involves the two electrons which are energetically closer.

 (iv) Each Auger transition proceeds with the unit probability to the nearest continuum limit. The decaying electron falls to a well-established $n$ level according to the energy equation.

 (v) If the new configuration still provides a multiple excited state involving more than two electrons, these rules are applied again until only two electrons remain bound to the projectile.

 (vi) If a particular cascading process leads to a highly asymmetric doubly excited state $(n_1, n_2 \geqslant 2n_1)$, the event is characterized as double radiative decay. Otherwise, if $(n_1, n_2 < 2n_1)$, a final Auger process takes place and the event is characterized as single charge exchange.

In  addition to this set of rules, the electronic angular momenta of the decaying electrons are determined throughout the Auger process by requiring the preservation of their respective orbital eccentricities. For the sake of simplicity, hydrogenic energy levels will be used to determine the projectile population after multiple charge exchange. This treatment is naturally expected to be more accurate as the projectile charge increases. Besides, the fact that this model retains the information on the angular momenta $(l)$ of the electrons throughout the Auger process turns unnecessary the use of *ad hoc* presupposed distributions for the angular

momentum, such as the flat distribution (where every $l$ subshell is evenly populated) or the statistical distribution (where the $m$ multiplicity is taken into account) to further process the subsequent radiative decay [28,41,42]. We note that a similar treatment involving three electrons has recently led to very good agreement with the Berlin-EBIT line emission cross sections for the $Ar^{18+}$ +Ar collision system [18,43].

Finally, in order to obtain emission cross sections, $\sigma_{n,l,m \to n',l',m'}^{(em)}$, cascade contributions from higher $n'' > n$ levels are added and the $n,l,m_l$ populations are multiplied by hydrogenic branching ratios $b_{l \to l'}$ for the relevant transitions [44] and by their relative line strength [38].

## III. RESULTS

### A. Total charge-exchange cross sections

In Fig. 3 we show the probabilities for a single electron in the 3s, 1p, and 2s orbitals to be captured by a projectile as a function of the impact parameter $b$. Projectiles charges $q = 6$ and $q = 10$ at a collision energy of 7$q$ keV are explicitly considered. At large impact parameters, the three models are in very good agreement. However, for lower impact parameters the SC and IA models predict almost identical distributions while mmCTMC departs and leads to slightly smaller probabilities. We relate this behavior to the simultaneous influence of both ionic centers on the captured electron, which is expected to be noticeable in the low $b$ range, in contrast to the SC and IA models for which the electron evolves subjected to a single ionic target core.

In Fig. 4, we show the resulting total charge-exchange cross sections $\sigma_{q,q-1}$ as a function of the projectile charge obtained by means of the mmCTMC, SC, and IA models. Fully stripped projectiles are considered only, and the experimental data of Mawhorter *et al.* [45] are included for comparison. We observe that the three models lead to results which are in
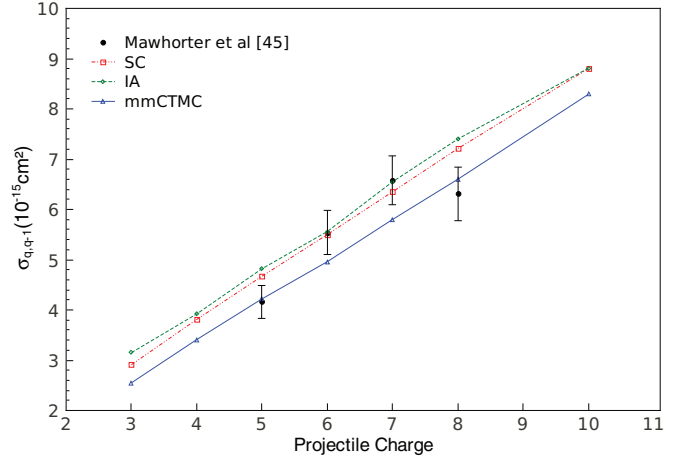


FIG. 4. (Color online) Single charge-exchange total cross section ($\sigma_{q,q-1}$) for fully stripped projectiles impinging on CO at 7$q$ keV. Results obtained with the mmCTMC (solid blue line with up triangles), SC (double-dotted-dashed red line with squares), and IA (dashed green line with down triangles) models are compared to the experimental data of Mawhorter *et al.* [45].

good agreement with the data, but while the SC and IA models are almost identical, those corresponding to the mmCTMC model are systematically lower in the projectile charge range considered.

Although this behavior is expected based on the capture probabilities shown in Fig. 3, to further clarify this point, in Fig. 5 we compare the average radial target potential seen by the electrons. For the multicenter potential, this average potential is provided by

$$V_{CO^+}(r) = \frac{1}{4\pi} \int d\Omega \, V_{CO^+}(r,\theta,\phi). \tag{6}$$
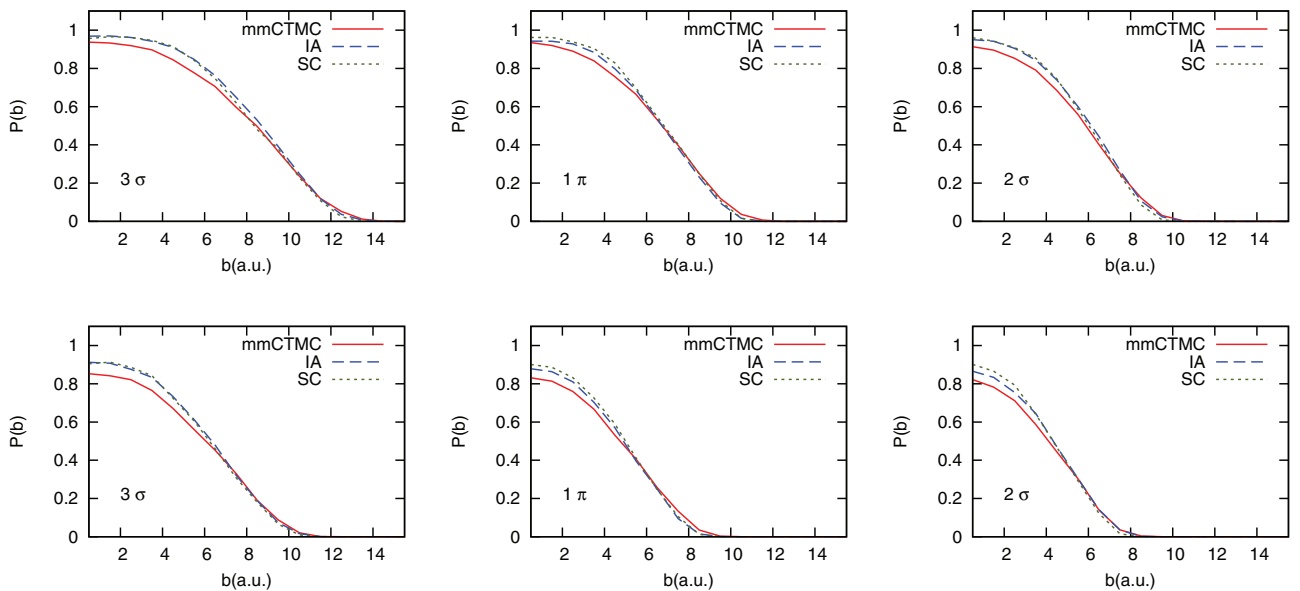


FIG. 3. (Color online) Capture probabilities by a projectile with to $q = 10$ (upper row) and $q = 6$ (lower row) of a single electron of the CO molecule originally in the 3$\sigma$ orbital, 1$\pi$ orbital, and 2$\sigma$ orbital. Results obtained with the mmCTMC (solid red line), SC (dotted green line), and IA (dashed blue line).
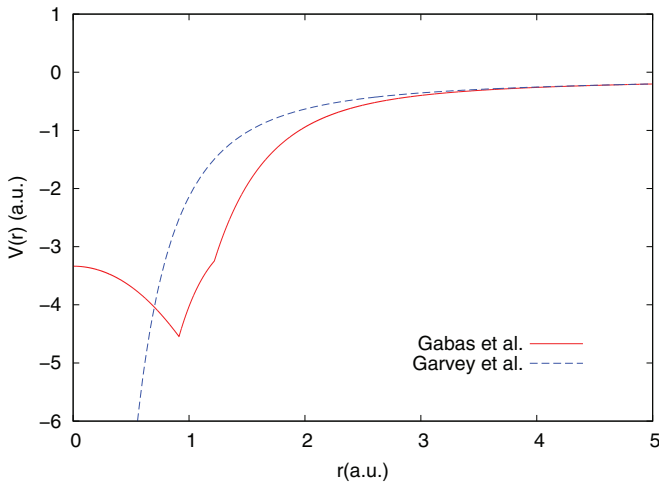
FIG. 5. (Color online) Average radial target potential seen by the electrons in the mmCTMC (red solid line) and SC (blue dashed line) models.

The origin in this plot coincides with the center of mass of the molecule. For the mmCTMC model $V_{CO^+}$ is given by the pseudopotential of Gabas *et al.* [Eq. (1)] and for the SC model we use the Garvey potential for $O^+$ [Eq. (2)]. As can be clearly observed, the molecular ion in the mmCTMC model shows a larger effective charge to the captured electron than the SC model for radial values (with respect to the molecular center of mass) greater than about 0.7 a.u.. As a result, a larger charge-exchange probability for the SC model compared to the mmCTMC model is expected. A similar comment applies for the IA model in which each electron sees at most a nuclear charge of $+6$ or $+8$ depending on the case orbital.

In Fig. 6, total double charge-exchange cross sections $\sigma_{q,q-2}$ are shown as a function of the projectile charge for the three models. These cross sections originate from multiple capture processes which lead to highly asymmetric doubly
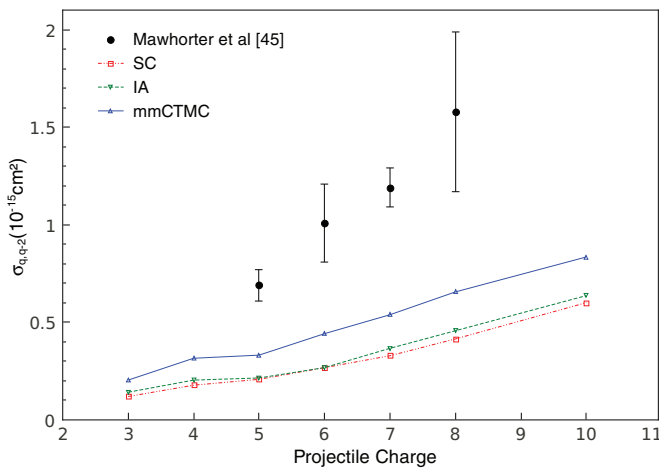


FIG. 6. (Color online) Double charge-exchange total cross section ($\sigma_{q,q-2}$) for fully stripped projectiles impinging on CO at $7q$ keV. Results obtained with the mmCTMC (solid blue line with up triangles), SC (double-dotted-dashed red line with squares), and IA (dashed green line with down triangles) models are compared to the experimental data of Mawhorter *et al.* [45].
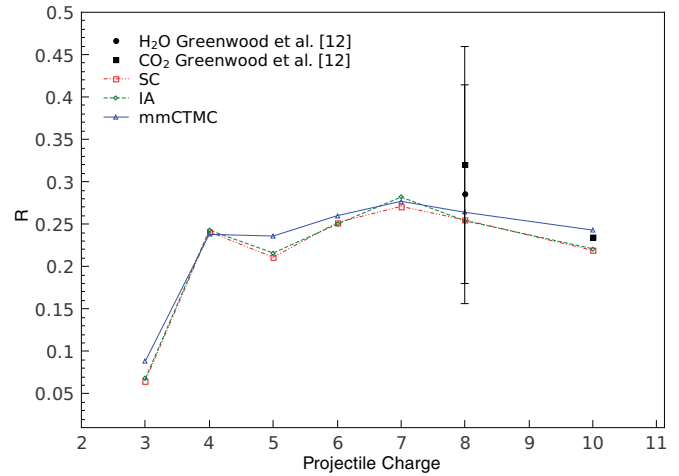


FIG. 7. (Color online) Hardness ratio ($R$) obtained with the mmCTMC (solid blue line with up triangles), SC (double-dotted-dashed red line with squares), and IA (dashed green line with down triangles) models compared to the experimental data of Greenwood *et al.* (Tables 3 and 4 of Ref. [12]) for $O^{8+}$ and $Ne^{10+}$ on $CO_2$ and $H_2O$ at a collision energy of $7q$ keV.

excited states. As can be inferred, the experimental data of Mawhorter *et al.* [45] are underestimated by the present models. Nevertheless, we note that the mmCTMC results are in better agreement with the data in the whole $q$ range explored.

### B. State-selective and line emission cross sections

We now compare the different models at the line emission and state-selective levels. In Fig. 7, we show the hardness ratio ($R$), which is defined as the line emission cross sections for the $np \rightarrow 1s$, $n > 2$, divided by that for the Lyman-$\alpha$ $2p \rightarrow 1s$ value, as a function of the projectile charge. From previous JPL data [11,12] with $O^{8+}$ and $Ne^{10+}$ projectiles, we infer that molecular targets of astrophysical interest such as $CO_2$ and $H_2O$, which have similar IP values, lead to almost identical line emission cross sections. We then expect that these $R$ values would represent good first-order estimates for CO as well, provided the similar IP. In Fig. 6, the experimental $R$ values from Ref. [12] are included to benchmark our theoretical results for projectile charges of $+8$ and $+10$. These results let us conclude that at an impact energy of $7q$ keV, x-ray emission spectra provided by the three models, as well as the data, will look much alike with a Ly-$\alpha$ line concentrating nearly 75% of the photonic emission during the radiative decay of the captured electron.

A much more demanding and stringent test is provided by the recent JPL data of Miller *et al.* [46] for the 36 keV $O^{6+} + CO$ collision system. In their work, the authors deconvolute from their spectra the relative state-selective population of the levels $n = 3$ and 4. These are presented in Table I together with the present theoretical results. As it can be seen, the theoretical results are in good agreement with the experimental data if the reported error bars are taken into account. The only disagreement is found in the $3s$ level, for which the three theoretical models tend to overestimate the experimental values by a factor of 3 or 4 depending on the case.

TABLE I. State-selective relative populations to $n = 3$ and $n = 4$ in 36 keV $O^{6+} + CO$ collisions. The experimental data correspond to Miller *et al.* [46].

|            | Expt.           | mmCTMC | SC    | IA    |
|------------|-----------------|--------|-------|-------|
| $4p$       | $0.13 \pm 0.03$ | 0.144  | 0.155 | 0.151 |
| $4d$       | $0.13 \pm 0.03$ | 0.089  | 0.096 | 0.096 |
| $4s$       | $0.23 \pm 0.05$ | 0.234  | 0.243 | 0.239 |
| $3p$       | $0.07 \pm 0.02$ | 0.117  | 0.102 | 0.105 |
| $3d + 4f$  | $0.41 \pm 0.09$ | 0.263  | 0.261 | 0.271 |
| $3s$       | $0.03 \pm 0.01$ | 0.154  | 0.144 | 0.138 |

Worth mentioning is that recent experimental data from KVI [13] for $O^{6+} + H_2O$ collisions at similar collisions energies exhibit a noticeably different behavior, with the $4s$ and $4p$ states being equally populated while the $3s$ state gets more populated than the $3p$ state. Provided the very similar line emission cross sections measured at JPL for molecular targets with similar IP values, such discrepancies at the state-selective level should be further explored. In particular, studies should be driven to check whether these discrepancies could be filtered during the cascade process. At the same time, this situation highlights the need of renewed theoretical efforts towards a more accurate description of molecular targets.

## IV. CONCLUSIONS

In this work we have presented a many-electron–multicenter CTMC model which we have tested in charge-exchange collisions between bare projectiles with charges $q = +3$ to $+10$ and CO. Other CTMC models based on the single-center approach for the molecule and the independent centers approach have been also used to benchmark the theoretical results of the this model.

These theoretical results have been compared to recent experimental data from JPL which include total charge-exchange cross sections, hardness ratios, and state-selective charge-exchange cross sections. The three models used in the present study compare well to the $\sigma_{q,q-1}$ cross sections (within error bars). Based on the predicted hardness ratios, we conclude that line emission cross sections should look alike for the three models used and are in agreement with the scarce data available.

In contrast to one-electron models, for which schemes based on binomial distributions must be recalled to account for multiple capture processes, the present many-electron treatment, married to the decay scheme developed by Ali, allows for a direct estimation of the autoionizing multiple capture contribution to the single charge-exchange channel. Besides, the fact that the angular momentum $l$ of the captured electron is explicitly considered along this procedure, avoids the need for invoking *ad hoc* functional forms for the $l$ distributions to further process the radiative decay. At this point, and provided the CO relevance in astrophysical environments, more state-selective data are urgently needed in order to help us theoreticians develop and refine more accurate descriptions of different molecular targets.

[1] T. E. Cravens, Science **296**, 1042 (2002).

[2] D. Bodewits, R. Hoekstra, B. Seredyuk, R. W. McCullough, G. H. Jones, and A. G. G. M. Tielens, Astrophys. J. **642**, 592 (2006).

[3] S. Otranto, R. E. Olson, and P. Beiersdorfer, Phys. Rev. A **73**, 022723 (2006).

[4] S. Otranto, R. E. Olson, and P. Beiersdorfer, J. Phys. B **40**, 1755 (2007).

[5] S. Otranto and R. E. Olson, Phys. Rev. A **77**, 022709 (2008).

[6] N. Djurić, S. J. Smith, J. Simcic, and A. Chutjian, Astrophys. J. **679**, 1661 (2008).

[7] J. Simcic, D. R. Schultz, R. J. Mawhorter, I. Cadez, J. B. Greenwood, A. Chutjian, C. M. Lisse, and S. J. Smith, Phys. Rev. A **81**, 062715 (2010).

[8] I. Abbas, C. Champion, B. Zarour, B. Lasri, and J. Hanssen, Phys. Med. Biol. **53**, N41 (2008).

[9] C. Champion, Phys. Med. Biol. **55**, 11 (2010).

[10] T. Liamsuwan and H. Nikjoo, Phys. Med. Biol. **58**, 641 (2013).

[11] J. B. Greenwood, I. D. Williams, S. J. Smith, and A. Chutjian, Phys. Rev. A **63**, 062707 (2001).

[12] J. B. Greenwood, I. D. Williams, S. J. Smith, and A. Chutjian, Astrophys. J. **533**, L175 (2000).

[13] D. Bodewits and R. Hoekstra, Phys. Rev. A **76**, 032703 (2007).

[14] P. Beiersdorfer, R. E. Olson, G.V. Brown, H. Chen, C. L. Harris, P. A. Neill, L. Schweikhard, S. B. Utter, and K. Widmann, Phys. Rev. Lett. **85**, 5090 (2000).

[15] P. Beiersdorfer, K. R. Boyce, G. V. Brown, H. Chen, S. M. Kahn, R. L. Kelley, M. May, R. E. Olson, F. S. Porter, C. K. Stahle, and W. A. Tillotson, Science **300**, 1558 (2003).

[16] H. Tawara, E. Takács, T. Suta, K. Makónyi, L. P. Ratliff, and J. D. Gillaspy, Phys. Rev. A **73**, 012704 (2006).

[17] R. Ali, P. A. Neill, P. Beiersdorfer, C. L. Harris, D. R. Schultz, and P. C. Stancil, Astrophys. J. Lett. **716**, L95 (2010).

[18] F. I. Allen, C. Biedermann, R. Radtke, G. Fussmann, and S. Fritzsche, Phys. Rev. A **78**, 032705 (2008).

[19] W. Fritsch and C. D. Lin, Phys. Rep. **202**, 1 (1991).

[20] N. Shimakura, S. Suzuki, and M. Kimura, Phys. Rev. A **48**, 3652 (1993).

[21] A. Salop and R. E. Olson, Phys. Rev. A **13**, 1312 (1976).

[22] A. Niehaus, J. Phys. B **19**, 2925 (1986).

[23] R. Abrines and I. C. Percival, Proc. Phys. Soc. London **88**, 873 (1966).

[24] R. E. Olson and A. Salop, Phys. Rev. A **16**, 531 (1977).

[25] C. Illescas, L. F. Errea, L. Méndez, B. Pons, I. Rabadán, and A. Riera, Phys. Rev. A **83**, 052704 (2011).

[26] C. J. Wood and R. E. Olson, Phys. Rev. A **59**, 1317 (1999).

[27] D. Greenspan, Phys. Scr. **52**, 267 (1995).

[28] T. Kirchner, M. Horbatsch, and H. J. Ludde, Phys. Rev. A **66**, 052719 (2002).

[29] A. Salehzadeh and T. Kirchner, J. Phys. B **46**, 025201 (2013).

[30] P. M. M. Gabas, L. F. Errea, L. Méndez, and I. Rabadán, Phys. Rev. A **85**, 012702 (2012).

[31] R. H. Garvey, C. H. Jackman, and A. E. S. Green, Phys. Rev. A **12**, 1144 (1975).

[32] R. S. Mulliken, J. Chem. Phys. **23**, 1833 (1955).

[33] C. L. Kirschbaum and L. Wilets, Phys. Rev. A **21**, 834 (1980).

[34] V. J. Montemayor and G. Schiwietz, Phys. Rev. A **40**, 6223 (1989).

[35] R. E. Olson, Phys. Rev. A **36**, 1519 (1987).

[36] W. M. Huo, J. Chem. Phys. **43**, 624 (1965).

[37] R. L. Becker and A. D. McKellar, J. Phys. B **17**, 3923 (1984).

[38] S. Schippers, P. Boduch, J. van Buchem, F. W. Bliek, R. Hoekstra, R. Morgenstern, and R. E. Olson, J. Phys. B **28**, 3271 (1995).

[39] J. Pascale, R. E. Olson, and C. O. Reinhold, Phys. Rev. A **42**, 5305 (1990).

[40] R. Ali, C. L. Cocke, M. L. A. Raphaelian, and M. Stockli, Phys. Rev. A **49**, 3586 (1994).

[41] R. Wegmann, H. U. Schimdt, C. M. Lisse, K. Dennerl, and J. Englhauser, Planet. Space Sci. **46**, 603 (1998).

[42] R. M. Häberli, T. I. Gombosi, D. L. De Zeeuw, M. R. Combi, and K. G. Powell, Science **276**, 939 (1997).

[43] S. Otranto and R. E. Olson, Phys. Rev. A **83**, 032710 (2011).

[44] H. A. Bethe and E. E. Salpeter, *Quantum Mechanics of One- and Two-Electron Atoms* (Springer, Berlin, 1957).

[45] R. J. Mawhorter, A. Chutjian, T. E. Cravens, N. Djurić, S. Hossain, C. M. Lisse, J. A. MacAskill, S. J. Smith, J. Simcic, and I. D. Williams, Phys. Rev. A **75**, 032704 (2007).

[46] K. A. Miller, W. W. Smith, T. Ehrenreich, Q. C. Kessel, E. Pollack, C. Verzani, V.A. Kharchenko, A. Chutjian, J. A. Lozano, N. Djuric, and S. J. Smith, Astrophys. J. **742**, 130 (2011).